



This work aims to investigate the temperature distribution of the study area by computing the brightness using the thermal infrared band of Landsat 8 data.

**MATERIAL AND METHODS**

Landsat 8 data for the scene covering the study area was downloaded from USGS website and ENVI software was extensively used for the entire procedure in this work which includes; radiometric calibration, at-satellite temperature calculation and brightness temperature calculation.

Image data may have either radiometric or geometric or both types of distortions. These distortions could be caused by sensor and plate, form errors during data acquisition. Therefore, before any analytical processing of satellite image, it has to be corrected for these distortions. This pre-processing operation is called image restoration or rectification (Thomas and Ralph, 1994).

The acquired Landsat 8 data was in the form of digital number (DN), necessitating its conversion to the top of the atmosphere (TOA) radiance otherwise known is radiometric calibration. This was done according to formulas from the

Landsat 8 Science Data Users Handbook using ENVI software. Equation 1 developed by the USGS was used to compute the spectral radiance from DN value of TIRS data of Landsat 8 (USGS, 2015).

$$L_{\lambda} = M_L Q_{cat} + A_L \tag{1}$$

$L_{\lambda}$  = Spectral radiance ( $W/(m^2sr\mu m)$ ).

$M_L$  = Radiance multiplicative scaling factor for the band (RADIANCE\_MULT\_BAND\_n from the metadata).

$A_L$  = Radiance additive scaling factor for the band (RADIANCE\_ADD\_BAND\_n from the metadata).

$Q_{cat}$  = Level 1 pixel value in DN.

The scene calibration data highlighted in table 1 below are essential for radiometric calibration. They are retrieved from the metadata file that was download with the Landsat8 scene.

**Table 1: LANDSAT 8 Radiance Scale Factors**

BAND NUMBER	$M_L$	$A_L$
BAND 10	3.3420E-04	0.10000
BAND 11	3.3420E-04	0.10000

**Sensor Brightness Temperature**

Brightness temperature (BT) is the microwave radiation radiance traveling upward from the top of Earth's atmosphere. To compute BT of an area the TOA spectral radiance of ( $L_{\lambda}$ ) is needed and has been calculated in equation 1 above. BT for both the TIRs bands was calculated by adopting the following formula (USGS, 2015):

$$T = \frac{K_2}{\ln\left(\frac{K_1}{L_{\lambda}} + 1\right)} \tag{2}$$

Where,  $K_1$  and  $K_2$  - thermal conversion constant which varies for both TIR bands (table 2)

$L_{\lambda}$  = Top of Atmospheric spectral radiance ( $Wm^{-2}sr^{-1}\mu m^{-1}$ ).

T = Top of Atmosphere Brightness Temperature, in Kelvin.

**Table 2: Thermal constant value of K1 and K2**

Thermal Constant	Band 10	Band 11
K1	774.8853	1321.0789
K2	480.8883	1201.1442

**RESULT AND DISCUSSION**

TOA radiance for TIR bands was calculated and the result is as shown in figure 2 a and b, and Table 3 highlights the statistic of the result.

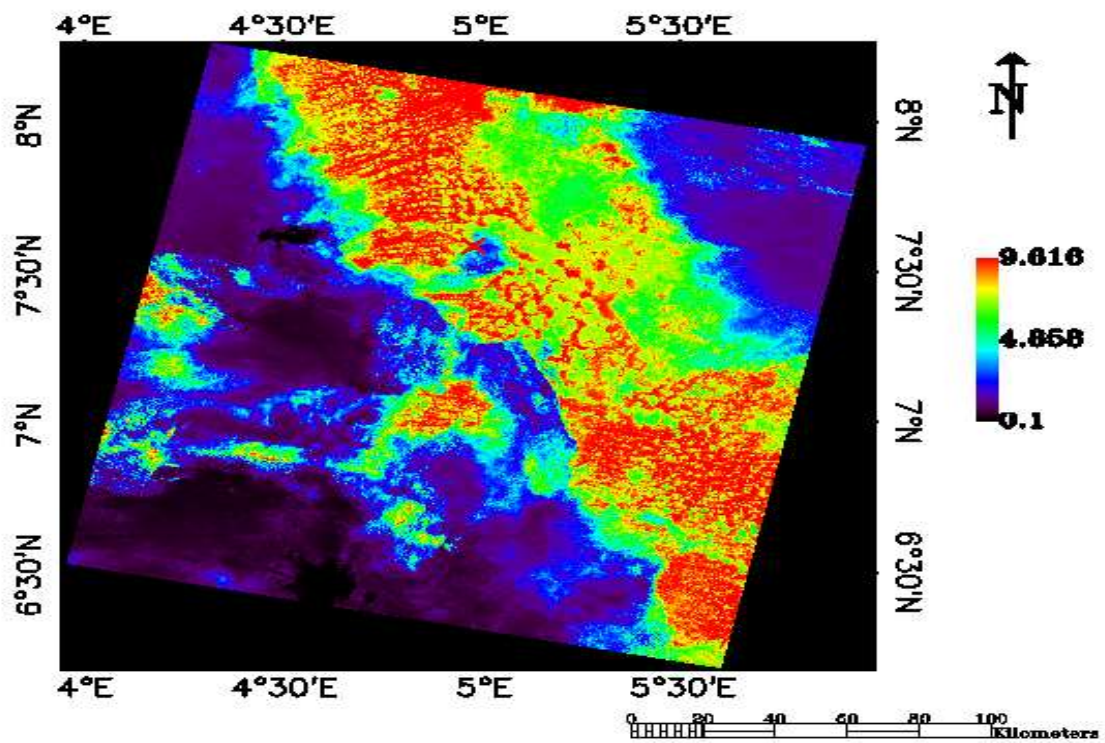


Figure 2 a: Radiance map of study area for band 10, the point mark X represents Ikogosi warm spring.

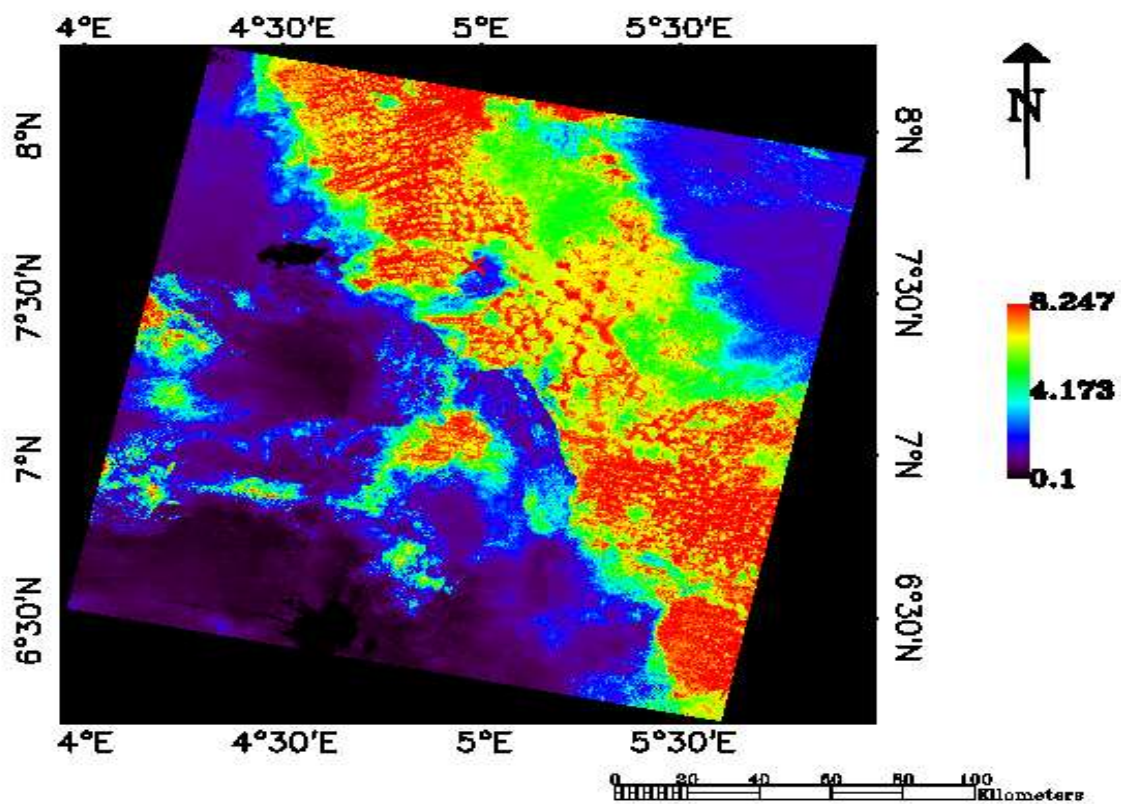


Fig. 2 b: Radiance map of study area for band 11, the point mark X represents Ikogosi warm spring.

**Table 3: Statistics of radiance for bands 10 and 11**

Band	Minimum	Maximum	Mean	SD
Band 10	0.100000	8.925220	4.505154	2.994511
Band 11	0.100000	7.782255	4.228131	2.782075

The geothermal manifestation within the study area is bordered by regions of high radiance while the vicinity is characterized by low radiance in both TIR bands. This could be occasioned by the presences of streams that source water from the springs. The result of brightness temperature computed for TIR bands 10 and 11 are as shown in figure 3 a and b below and the statistics of the result is shown in table 4 below.

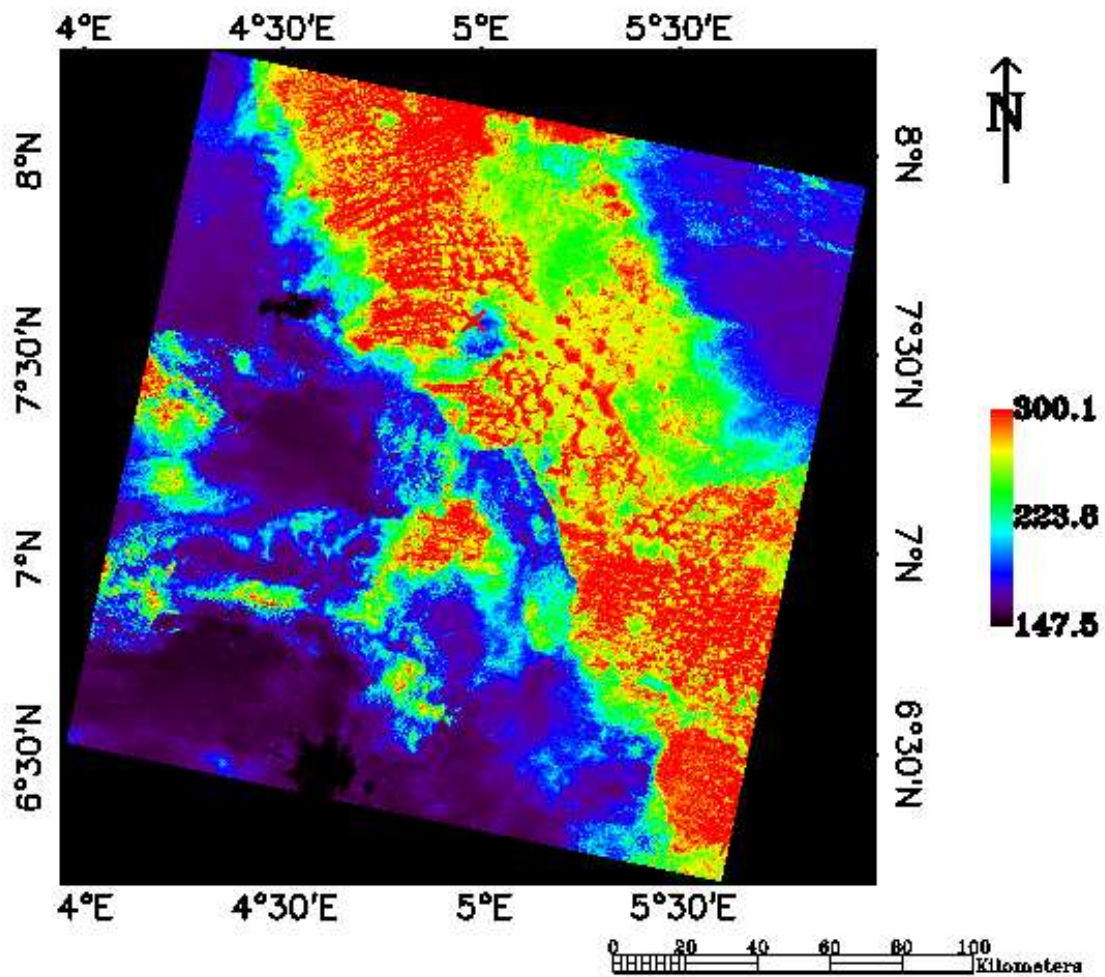


Fig. 3 a: Top of Atmosphere Brightness Temperature map for band 10, the point mark X represents Ikogosi warm spring.

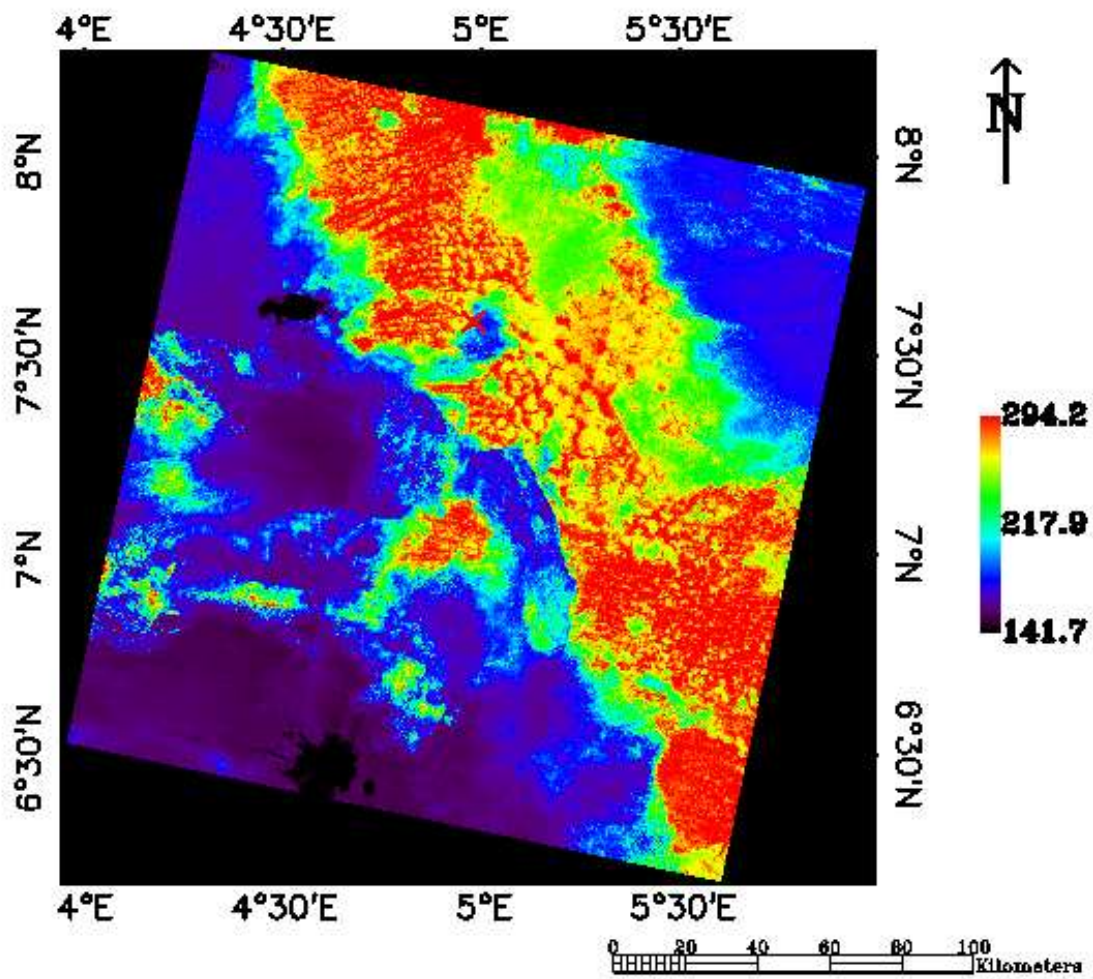
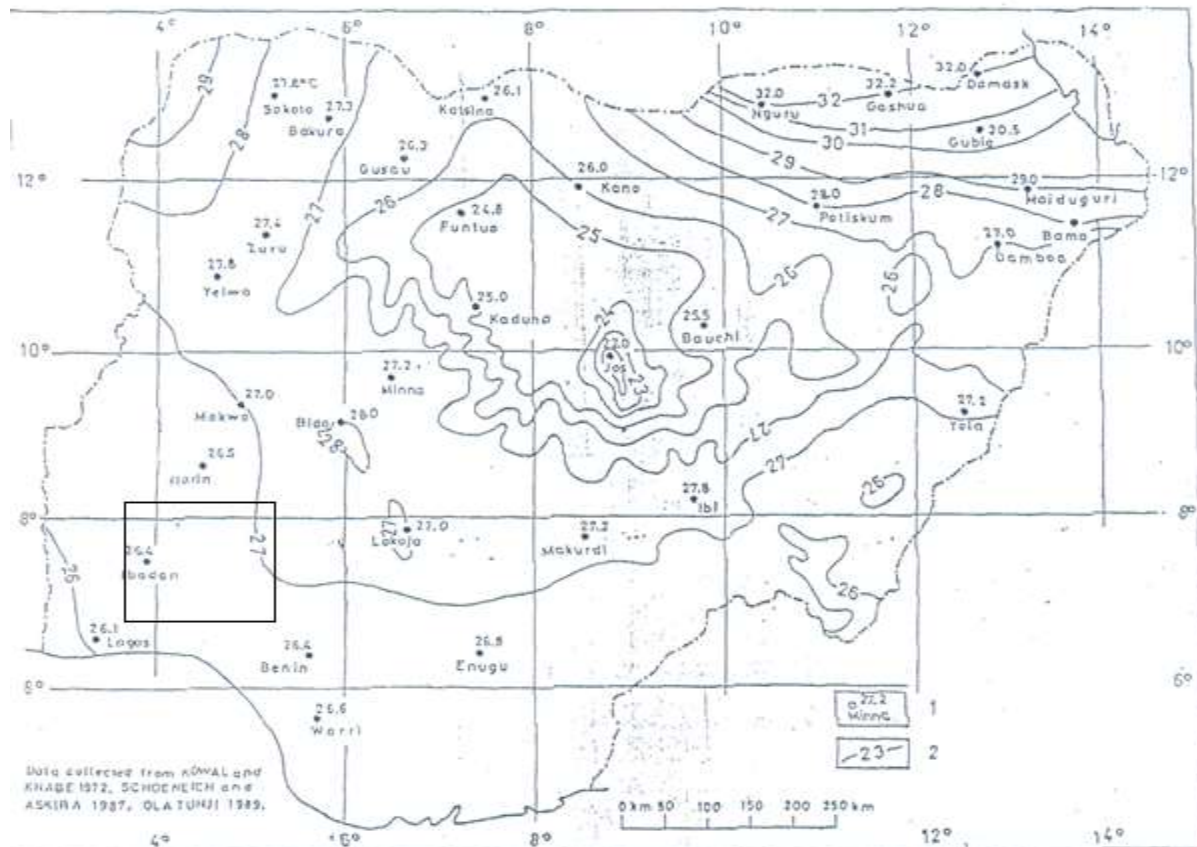


Figure 3 b: Top of Atmosphere Brightness Temperature map for band 11, the point mark X represents Ikogosi warm spring.

Table 4: Statistics of brightness temperature for bands 10 and 11

Band	Minimum	Maximum	Mean	SD
Band 10	147.517090 K	300.137115K	239.398301 K	61.509098 K
Band 11	141.670624 K	294.195160 K	236.134609 K	63.182204 K

Regions around the geothermal manifestation are of high temperature most especially the NW and SE of the warm spring. The result was compared with a map of annual average ground surface temperature (figure 3) and it was observed that the temperature distribution pattern is in agreement thereby validating the result of the brightness temperature.



Fig/ 4: Map of annual average ground surface temperature (After Schoeneich 1998). The square box represents the study area.

## CONCLUSION

The result of the computed brightness temperature for the thermal band, which ranges from 141 K 300 K, indicates that temperature decreases along SW direction of the study area and it in concordance with the average ground surface temperature.

It was also observed that regions around the Ikogosi is of temperature above 290 K while that of the vicinity is about 200 K and it could be due to the stream in the vicinity.

## REFERENCES

- Caby, R., & Boessé, J. M. (2001). Pan-African nappe system in southwest Nigeria: The Ife-Ilesha schist belt. *Journal of African Earth Sciences*, 33(2), 211–225. [https://doi.org/10.1016/S0899-5362\(01\)80060-9](https://doi.org/10.1016/S0899-5362(01)80060-9)
- Chan, H., Chang, C. and Dao, P.D. (2018). Geothermal Anomaly Mapping Using Landsat ETM+ Data in Ilan Plain, Northeastern Taiwan. *Pure Applied Geophysics*, 175, 303–323. <https://doi.org/10.1007/s00024-017-1690-z>
- De Swardt, A. (1953). “The geology of the country around Ilesha”, *Geological survey Nigeria Bulletin*, 28: 54.
- Gaudin, D., Beauducel, F., Allemand, P., Delacourt, C., and Finizola, A. (2013). Heat flux measurement from thermal infrared imagery in low-flux fumarolic zones: example of the Ty fault (La Soufrière de Guadeloupe). *Journal of Volcanology and Geothermal Research*, 267, 47–56.
- Gutiérrez, F. J., Lemus, M., Parada, M. A., Benavente, O. M., and Aguilera, F. A. (2012). Contribution of ground surface altitudedifference to thermal anomaly detection using satellite images: application to volcanic/geothermal complexes in the Andes of Central Chile. *Journal of Volcanology and Geothermal Research*, 237–238, 69–80.
- Thomas, M. L. and Ralph, W. K. (1994). *Remote Sensing and Image Interpretation*, 3rd ed., John Wiley and Sons, New York, 750
- USGS (United State Geological Survey) (2015). Landsat 8 Data User Handbook. Retrieved from <http://landsat.usgs.gov> accessed on January 30, 2016.
- Wu, W., Zou, L., Shen, X., Lu, S., Su, N., Kong, F., et al. (2012). Thermal infrared remote-sensing detection of thermal information associated with faults: a case study in Western Sichuan Basin, China. *Journal of Asian Earth Sciences*, 43, 110–117